

THESIS FOR THE DEGREE OF LICENTIATE OF ENGINEERING

Mechanistic aspects of structure and dynamics in perovskite type oxyhydrides and alkali silanides

CARIN ÖSTERBERG



CHALMERS

Department of Physics

CHALMERS UNIVERSITY OF TECHNOLOGY

Gothenburg, Sweden 2016

**Mechanistic aspects of structure and dynamics in perovskite type
oxyhydrides and alkali silanides
CARIN ÖSTERBERG**

© CARIN ÖSTERBERG, 2016

Department of Physics
Chalmers University of Technology
SE-412 96 Göteborg, Sweden

Chalmers Reproservice
Göteborg, Sweden 2016

Mechanistic aspects of structure and dynamics in perovskite type oxyhydrides and alkali silanides

Carin Österberg
Department of Physics
Chalmers University of Technology
SE-412 96 Göteborg, Sweden

Abstract

This Thesis concerns experimental studies of the two alkali silanides $ASiH_3$ ($A = K$ and Rb) and the recently discovered perovskite type oxyhydrides $BaTiO_{3-x}H_x$ ($x = 0.14$ and 0.40). The alkali silanides $ASiH_3$ ($A = K$ and Rb) are featured by an unusually low enthalpy change over the hydrogen absorption/desorption process, which enables an easy route for hydrogenation and makes them of relevance for hydrogen storage applications. One aim with this thesis is to determine the mechanistic aspects of the structure and hydrogen dynamics that possibly explain this behavior. It is shown that the previously reported structure, featured by a quasi-spherical arrangement with 24 sites of preferred orientations for the hydrogen atoms, can be used as a model for the H dynamics present in the materials. Specifically, the SiH_3^- species are almost freely rotating, which explains the origin of the low entropy variation.

Perovskite type oxyhydrides $BaTiO_{3-x}H_x$ ($x = 0.14$ and 0.40) represent an emerging class of hydride-ion conducting materials, with properties similar to proton conducting equivalents. However, details of the hydride-ion dynamics are still unknown. Accordingly, this thesis focuses also on investigations of the mechanistic aspects of structure and hydride-ion dynamics in perovskite oxyhydrides, with the aim of developing a generic knowledge of hydrogen dynamics in perovskite materials, relevant for both proton and hydride-ion conductors. Structural and dynamical analysis confirm that the hydride-ions are located on vacant oxygen sites of the perovskite lattice and reveal hydride-ion diffusion on the time-scale of nanoseconds.

The main means of investigation are neutron scattering techniques, which are very appropriate in order to study hydrogen dynamics in materials. This will be discussed in detail in this thesis and also the basics of dynamics that is at the center of the investigations.

Keywords: *energy materials, hydrogen dynamics, localized motion, oxyhydride, quasielastic neutron scattering, inelastic neutron scattering, mean square displacement*

Publications included in this thesis

I Dynamics of Pyramidal SiH_3^- Ions in ASiH_3 ($A = \text{K}$ and Rb) Investigated with Quasielastic Neutron Scattering

Carin Österberg, Henrik Fahlquist, Ulrich Häussermann, Craig M. Brown, Terrence J. Udovic, Maths Karlsson

Journal of Physical Chemistry C **120**, 6369-6376 (2016)

II A neutron scattering study of the hydride-ion dynamics in the novel perovskite oxyhydrides $\text{BaTiO}_{3-x}\text{H}_x$ ($x = 0.14$ and 0.4)

Carin Österberg, Reji Nedumkandathil, Ulrich Häussermann, Madhusudan Tyagi, Craig M. Brown, Stewart F. Parker, Maths Karlsson

In manuscript

The author's contributions to the papers:

I The author did the QENS experiments, the analysis, wrote the first draft and was the main author.

II The author did the QENS experiments, the analysis of both the QENS and the INS data, wrote the first draft and was the main author.

Contents

1	Introduction	1
2	General aspects of hydrogen dynamics in materials	3
2.1	Vibrational motions	3
2.2	Localized diffusional motions	5
2.3	Long-range translational diffusional motions	7
3	Hydrogen in Alkali Silanides and Oxyhydrides	11
3.1	Alkali Silanides	11
3.2	Perovskite Oxyhydride	14
4	Neutron scattering techniques	19
4.1	Neutron diffraction	20
4.2	Inelastic neutron scattering	22
4.3	Quasielastic neutron scattering	24
5	Instrumentation	31
5.1	The DCS quasielastic spectrometer	32
5.2	The HFBS quasielastic spectrometer	32
5.3	The TOSCA inelastic spectrometer	33
5.4	The D2B diffractometer	34
6	Summary of appended papers	35
7	Conclusions and outlook	37
	Acknowledgments	39

Bibliography	41
Papers I-II	47

Glossary

CMP	Condensed Matter Physics
DCS	Disk Chopper Spectrometer
EISF	Elastic Incoherent Structure Factor
ESS	European Spallation Source
FWHM	Full Width at Half Maximum
FWS	Fixed Window Scan
HFBS	High Flux Backscattering Spectrometer
ILL	Institut Laue-Langevin
INS	Inelastic Neutron Scattering
MSD	Mean-Square Displacement
NIST	National Institute of Standards and Technology
NCNR	NIST Center for Neutron Research
P-T window	Pressure-Temperature window
QENS	Quasielastic neutron scattering
RT	Room Temperature

1

Introduction

The concept of energy materials is getting more and more an important subject of discussion and research due to the large demand of finding the next generation of energy storage and conversion. This thesis focuses on investigations of the fundamental aspects of hydrogen atoms and their motions (dynamics) in two important classes of energy materials, alkali silanides and perovskite type oxyhydrides, with the aim to develop important fundamental insight of how to design new and more efficient energy materials for the future.

Since the world is shifting towards a more hydrogen based economy, research of various aspects of hydrogen in matter is becoming increasingly important.[1–4] A simple method to produce hydrogen gas is through splitting of water, which can be used to store energy, *i.e.* if the water is split with wave energy, the resource and materials are then provided in a very close proximity and would lower transportational costs and energy loss due to the distance between production and demand.[5–7]

But how to store the hydrogen in a safe, efficient and economical way? A good candidate for this challenge is the storage of hydrogen in a solid material. At a first glance this might be seen as a more complicated way to store hydrogen compared to how it is done presently in, for example, cars, where it is stored in gaseous form, in a pressurized tank.[8] However, considering the extra energy that is put to pressurize the hydrogen gas and also depressurizing it during use, a good alternative would be to reduce the number of steps and have the hydrogen storage medium working under mild pressure (close to atmospheric pres-

sure) and temperature (close to room temperature) instead.[9, 10] This could be possible with a solid storage exhibiting both easy absorption/desorption and a high concentration of hydrogen inside the material.[11] These characteristics, especially absorption/desorption, are widely governed/affected by the dynamical behavior of the hydrogen atoms within the material. However, for many materials the hydrogen dynamics are relatively unknown and therefore in which way the hydrogen dynamics correlate to hydrogen storage characteristics is still not fully understood.[12, 13]

The mechanistic aspects (*i.e.* the time-scale, activation energy, and spatial geometry) of hydrogen diffusion through many materials is still relative unknown and the different processes in which this could happen are a sea of vast possibilities. The most commercial way to promote a hydrogen economy, is through fuel cell vehicles. This would be a good substitute for the combustion engine in the cars of today, in order to avoid the hazardous exhaust that presently is polluting our air and environment. To obtain the fuel cell as efficient as possible, one crucially important feature is a high mobility of the hydrogens through its, so called, electrolyte. However, in most currently available materials, the mobility of hydrogen ions (protons) is too low. Developing new highly conductive materials depends on an increased understanding of the mechanistic aspects of hydrogen dynamics in present-day materials, as well on the exploration of new systems.[8, 14–16]

In this Thesis, the dynamical behavior of two technically relevant materials, alkali silanides and perovskite type oxyhydrides, is investigated. The primary tools for these investigations involve the use of different neutron scattering techniques, which are particularly powerful for studies of hydrogen and hydrogen-based materials.[17] Upon shooting neutrons on materials and analyzing the properties of the scattered ones, a wide range of information about structure and dynamics can be obtained. This information may then be used to explain the properties described above and help to identify new materials optimum for the applications mentioned.

2

General aspects of hydrogen dynamics in materials

Hydrogen dynamics play a key role in many materials and for their functional properties, such as conduction, heat capacity or gas exchange, for example. Generally, the dynamical behavior of materials may be divided into three classes of motions; vibrational, localized diffusional, and long-range translational diffusional. These are described more in the following.

2.1 Vibrational motions

Vibrational motions occur on the shortest time-scale of ps-fs and give information about the structure and nature of bonds within a material.

Vibrational modes give rise to bands throughout most of the infrared region of the electromagnetic (radiation) spectrum. Usually when a vibrational spectrum is presented the vibrational bands are showed with the wavenumber ($\bar{\nu}$), expressed in cm^{-1} . The unit cm^{-1} is the number of waves in a 1 cm-long wavetrain, which might not say that much, but the unit is related to other parameters by,

$$\bar{\nu} = \frac{\nu}{(c/n)} \qquad \bar{\nu} = \frac{1}{\lambda}.$$

Here is ν the frequency (the number of vibrations per unit time) and λ , the

wavelength of the electromagnetic radiation, whereas c is the velocity of light in vacuum and n is the reflective index of the medium in which the wavenumber is measured. However, wavelength is a property of radiation and not of molecules. But, radiation and molecules do have the properties energy and frequency in common. The photon energy (used to measure the vibrational motions of the material) may be absorbed or emitted by a molecule, in which case the vibrational energy of the molecule will be changed by ΔE_v , following the principle of conservation of energy,

$$\Delta E_v = E_p = h\nu = hc\bar{\nu}. \quad (2.1)$$

The photon energy is represented by E_p , h is Planck's constant and ΔE_v can be either positive or negative depending on if the photon is absorbed or emitted, respectively. More importantly, $h\nu$ is the energy of the vibration. [18] In general, the smaller the reduced mass of the vibrating unit is and the stronger the bond is, the higher is the vibrational frequency.

A phonon is when the lattice of the materials vibrates, which usually exhibits a lower vibrational frequency. To describe the phonon, a simplified model for a crystal can be used, where a chain of atoms with a mass is placed regularly and they are all connected with springs. In this manner, when the crystal is influenced by thermal motions, they will spread through the material as mechanic waves. These can be described as propagating waves or as particles with a given energy ($h\nu$) and momentum, hence a phonon. For low frequencies, the velocity of the wave is equal to the speed of sound in the material and is therefore called an *acoustic phonon*. The acoustic phonons correspond to a more simple and one dimensional structure as the simplified model. Whereas if the phonon propagates through a material consisting of atoms of different weight or bond potential, where the bonds show a much higher deformation, the frequencies will be higher and show *optical phonons*. Furthermore, both of these cases of phonons, acoustic and optical, can exist as *longitudinal* or *transverse* ones. The difference between these is that the atomic displacement has a direction, which can be either parallel or perpendicular to the wave vector \mathbf{q} ¹ and hence be longitudinal and transverse, respectively. For a simplified model

¹will be discussed further in Chapter 4

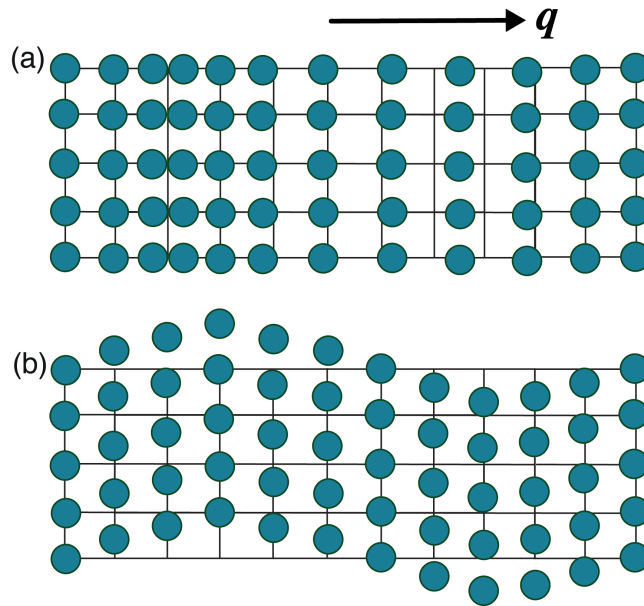


Figure 2.1: A simplified model of (a) longitudinal and (b) transverse waves.

of this see Fig. 3.1.[19, 20]

2.2 Localized diffusional motions

It might be peculiar to discuss about molecules when investigating a solid and not a liquid or gas, even though there is an important material to discuss when it comes to dynamics, the plastic crystals. The characteristics of a plastic crystal is that the molecules have their centers of mass well located in space on a crystalline lattice, but their orientations vary from one site to the other and change with time. Nonetheless, the sites of the molecular reorientations are on distinguished equilibrium positions so that the lattice still establish generally high symmetry. This is usually due to the weak van der Waals' forces reflecting both the symmetry of the molecule and the surroundings, building up an intermolecular potential. Hence, the radial part of the potential is responsible for the translational order, whereas the angle-dependent part of the potential is controlled by the orientational ordering of the molecules. More specifically, the angular motions are governed by an orientational crystal field, whose potential exhibits minimas at the equilibrium orientations. Potential barriers exist

between these preferred positions and the orientational motions can be classified by the height of the hindrance potential. Basically, there are two main situations for the height of the hindrance potential relative to the rotational constant, $\hbar/2I$ (where I is the moment of inertia); one where the height is large compared with the rotational constant, and the other where the height is instead small in comparison.

In the first case, the molecule is captured in the orientation that corresponds to the minima of the potential, where it performs small angular oscillations around the orientation with high frequency (librations). When the temperature goes above a specific limit for the material, thermal excitations of the molecule will then be of the same order of magnitude as the rotational constant. Hence, the molecule can jump over the barrier to another preferred orientation and a jump diffusion occurs. The time, τ , can then be used for a measure of the average time the molecule spends between jumps, where τ follows an Arrhenius law,

$$\tau = \tau_0 \exp(E_a/k_B T). \quad (2.2)$$

Here, E_a is the activation energy, *i.e.* the difference between the height of the potential and the librational ground state energy. Realistically, the jump motion probably happens continuously, but the number of molecules participating is fewer than the molecules in the minimas, which makes the average diffusion look like there is an average time between jumps.

In the second case, at the high temperature limit, the potential barrier shows large fluctuations, resulting from interactions between the rotations and the thermal lattice vibrations or by reorientations of neighboring molecules. This, instead, results in a rotational diffusion, where the molecule rotates continuously without any preferred orientations in space. Nevertheless, there are some unsatisfactory details with both the jump model and the rotational diffusion model. The former sets the angular displacements of the rotational to very specific trajectories for each atom and no deviations are allowed. The second ignores the fact that there is actually preferred orientations of the molecule that could influence the probabilities of the diffusion.

In the following are shown some examples of the models describing the two cases above. The simplest case for an atom that jumps within a limiting space,

is the so called dumbbell model, where the atom jumps forth and back between two isoenergetical sites.² Another model to consider is when the atom jumps between three sites on a circle, which could be adapted for jumps between 4, 5, 6 sites and so on. For rotational diffusion, one important model is the isotropic rotational diffusion model, which describes the free (random) diffusion of atoms around a central atom. Over a time average the molecule will then build up a sphere of atomic positions with the radius of the bond length between the diffusing atom and the central atom. Moreover, if the molecule is somewhat more restrained, the rotational diffusion can be described with a continuous rotational diffusion on a circle. This model is built on the jump model between sites on a circle, but where the number of sites, N , is so big so that the diffusion can often be approximated as continuous.[21, 22] If the temperature is increased for a material that exhibits molecular reorientations, the thermal energy can become high enough to make the atoms leave the localized space it occupies and diffuse on a longer length-scale. This will be discussed in the next section.

2.3 Long-range translational diffusional motions

Diffusion in crystalline solids usually occurs due to the presence of point defects, such as vacancies or interstitials. But it can also take place along 1- and 2-dimensional defects, such as dislocations, grain boundaries and surfaces. The parameters which control the type of diffusion that possibly occur is temperature, partial pressure and other characteristics, such as the microstructure, grain size, porosity of the sample. For example, lattice diffusion usually has a larger activation energy compared to grain boundary diffusion, which often restricts this kind of diffusion to higher temperature.[21–24]

When describing a diffusional process, the solid ground to stand on is Fick's first law, which simply describes the flow of particles from high to low concentrations:

$$j = -D \frac{dc}{dx}, \quad (2.3)$$

where j is the particle flux density, $\frac{dc}{dx}$ the concentration gradient of particles and D the diffusion coefficient. This fairly simple equation can be modified

²This and the other models will be explained further in chapter 3

to include either an electrical or chemical potential gradient for electrically charged or neutral particles, respectively. In reality though, it can often be a combination of both, which makes the equation a bit more complicated and often it is instead treated as an approximation.

Two vital parameters of diffusion that here need to be described are the jump frequency (Γ) and the jump distance (l), which are connected to each other by the following equation:

$$j = -\frac{1}{2}l^2\Gamma\frac{dc}{dx}. \quad (2.4)$$

The factor $\frac{1}{2}$ denotes that the equation only applies to one-dimensional jumping particles, hence only half of the particles jumps in the considered direction. To describe the possibility of three-dimensional jumps, $\frac{1}{3}$ of the particles will have the possibility to diffuse along one of three orthogonal directions, that is $\frac{1}{3}$ of the flux in one direction of the flux as described before, which gives the factor $\frac{1}{6}$,

$$j = -\frac{1}{6}l^2\Gamma\frac{dc}{dx}. \quad (2.5)$$

Combining the above equation with Fick's first law (Eq. 2.3) gives an expression for the diffusion coefficient D in three dimensions,

$$D = \frac{1}{6}l^2\Gamma. \quad (2.6)$$

Additionally, considering a large number of jumps (n) and a time (t) for which the jumps occur gives

$$\Gamma = \frac{n}{t}. \quad (2.7)$$

Combining Eq. 2.7 with Eq. 2.6 one (eventually) obtains,

$$nl^2 = 6Dt. \quad (2.8)$$

The factor 6 denotes a three-dimensional diffusion, but this can be changed to 4 or 2, for two-dimensional and one-dimensional diffusion, respectively. The parameters in Eq. 2.8 are useful when getting the full picture of a diffusional process in a material. The distance l should correspond to a reasonable length in the structure/lattice of the material in order to verify the analysis of the

results. Also the time (t) between jumps should be within reasonable limits, a too short time could imply that the process detected is not in fact a diffusional process but rather a vibrational one.[21–25]

However, Fick's law generates only a simple long-range diffusional model, which is only true for weak interparticle interactions and very small random displacements. To expand this description and include more complicated long-range diffusional models, there is a number of additional terms and models to consider. This could compensate for when the strength of the interparticle interactions increases or when the time for the particle at rest is much longer than the jump time. There are, of course, several more variants of long-range diffusion, for some of which mathematical models have been developed. The kind of dynamical motion the material exhibits will influence, and in many cases explain the properties of materials.[21]

3

Hydrogen in Alkali Silanides and Oxyhydrides

3.1 Alkali Silanides

Currently, there is a large effort devoted to the development of technologies that use hydrogen as an energy source, specifically for fuel-cell applications. A specific challenge is to design a hydrogen storage material that is safe, economic and efficient.[26, 27] The specific demands on the material is that the hydrogen exchange must take place under mild pressures and at temperatures close to room temperature (RT), in order to connect well with the rest of the fuel cell system. To meet these demands one approach is to develop a thorough understanding of the dynamical behavior of hydrogen in promising materials, and on that ground develop materials that mimic the properties of a gas.

The expanding list of promising materials for hydrogen storage applications include materials such as amides $M(\text{NH}_2)_x$, imides $M(\text{NH})_{x/2}$, borohydrides $M(\text{BH}_4)_x$, alanates $M(\text{AlH}_4)_x$ and $M_x(\text{AlH}_6)_y$, which are already well investigated in the literature, and also the recently investigated amido-boranes $M(\text{NH}_2\text{BH}_3)_x$, ammonium-closo-borane $(\text{NH}_4)_2\text{B}_{12}\text{H}_{12}$ and hydrazinido-boranes $M(\text{N}_2\text{H}_3\text{BH}_3)_x$. [28–40]. Recently, it has been shown that the hydrogenation of the ASi ($A = \text{K}, \text{Rb}$ and Cs) Zintl phases gives alkali metal silyl hydrides ASiH_3 ($A = \text{K}, \text{Rb}$ and Cs), which are able to store up to 4.3, 2.6 and 1.85 wt. % of H_2 , respectively. Additionally, the hydrogenation process is reversible in a

good P - T window; a 0.1 MPa hydrogen equilibrium pressure can be obtained at around 414 K, which is compatible with proton exchange membrane (PEM) fuel-cell applications.[11, 12]

At room temperature, the crystal structure of $ASiH_3$ corresponds to an average cubic NaCl-type arrangement of alkali metal and Si atoms, meaning that pyramidal SiH_3^- anions are distributed in random orientations in the crystal structure (α - $ASiH_3$).[12, 41, 42] At temperatures below 200 K, $ASiH_3$ compounds exist as hydrogen-ordered β modifications.[11–13, 43] On the basis of differential thermal analysis on $KSiH_3$, a reversible phase transition was observed between the high-temperature α -phase and low-temperature β -phase on cooling (273–278 K) and the reverse (β to α) on heating (288–293 K), thus indicating some hysteresis in the material.[43] The favorable thermodynamic characteristics of α - $ASiH_3$ is due to an unusually low entropy variation over the hydrogen absorption/desorption process. This has been attributed to the disorder in α - $ASiH_3$, whose structural properties actually correspond close to that of a slightly compressed gas-phase species (Si-H bond length = 1.52 Å; H-Si-H angle 92.2°). In an attempt to describe the dynamics of this material, a good starting point is the structure, which suggests a quasi-spherical arrangement with 24 sites of preferred orientations for the hydrogen atoms around each Si atom (Fig. 3.1). This means that a reorientation model needs to be considered, that do not necessarily preserve a particular orientation of the SiH_3^- ions in the NaCl-type crystal structure, but in fact could describe a jump diffusion on the surface of a sphere, with 24 different jump locations. This model represents a combination of rotational diffusion motion and localized jump diffusion. Thus, the model is similar to the isotropic rotational diffusion model, with the molecule free to reorient in any direction, but still includes small jump distances to preferred hydrogen sites.[12, 13, 43]

Through the analysis of neutron scattering data of $ASiH_3$ ($A = K$ and Rb) performed in this thesis, the 24 site model was confirmed and more could be understood about both the structure and dynamics of $ASiH_3$ ($A = K$ and Rb). For example, the effect of the type of alkali ion on the SiH_3^- dynamics could be attributed to the difference in atomic radii between the two ions, K (152 pm) and Rb (166 pm),[45] where the slightly more spacious structure of $RbSiH_3$ favors the earlier onset of dynamics. Besides being of considerable

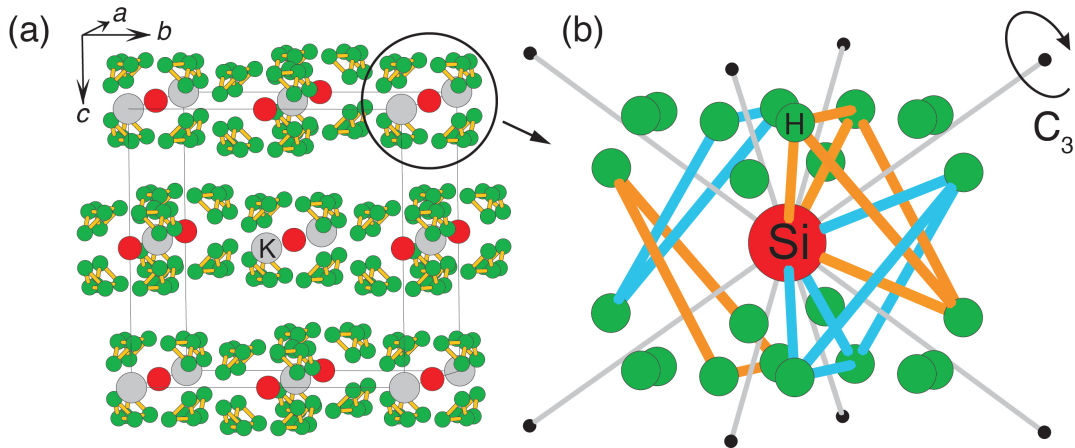


Figure 3.1: (a) Structural model for disordered α -KSiD₃ representing a cubic NaCl-type arrangement of K and Si atoms (space group $Fm\bar{3}m$). H atoms distribute according to a $96k$ Wyckoff site (occupancy 12%). This yields a quasi-spherical environment of 24 H atom positions around each Si atom. (b) The 24 H atom environment as a consequence of aligning pyramidal SiH_3^- ions (with respect to their C_3 axis) randomly along the four body diagonals of the cubic unit cell (grey lines). This yields eight possible orientations of which four (two "up" and "down" alignments) are emphasized in the figure (light blue and orange bonds). The figure is reproduced from Paper I.[44]

fundamental interest, increasing the understanding of the nature of the SiH_3^- orientational mobility in the disordered phases of KSiH_3 and RbSiH_3 , may explain the high entropy observed in the α -phase resulting in the low entropy variation for hydrogen absorption/desorption and hence the origin of these materials' favorable hydrogen storage properties.

An interesting comparison to ASiH_3 is the related material LiBH_4 , which shows a favorable hydrogen mass fraction (0.185), but a somewhat unfavorable hydrogen-cycling behavior.[32] Efforts have been made to put this molecule in different confinements to improve the thermodynamics, kinetics and reversibility of hydrogen absorption/desorption in LiBH_4 . These confinements have consisted of different solutions such as nanopores, mixing with MgH_2 , and mixing with Li halide salts. This is therefore done to change the localized dynamical behavior. Compared to the dynamical behavior of hydrogen in ASiH_3 , where the hydrogen atoms diffuse between 24 sites on a sphere, the rotational behavior of T_d BH_4^- ions in cubic ABH_4 phases involves a much more easily realized

dynamics of rotational jumps of the molecules about the high-symmetry axes. It involves 90° reorientations around the three C_2 axes (resulting in a cubic H environment around the B atoms) and 120° rotations around the four C_3 axes.[34] In a structure like this, the reorientations around any particular axis are very rapid but a jump reorientation of the entire axis are usually much slower. This may be related to the unfavorable thermodynamic behavior that bulk LiBH_4 exhibits compared to ASiH_3 . However, when LiBH_4 is instead put in a nanoconfinement of carbon scaffolds, the molecular reorientations change and go from localized jump motions to an uniaxial rotational diffusion.[35] This motion is much closer to the motion suggested for ASiH_3 , and hence the thermodynamic behavior changes for LiBH_4 and the hydrogen absorption/desorption process is improved.[32–35, 46] This shows how the knowledge about the dynamical behavior of the reorienting molecule can help to design new, improved hydrogen storage materials.

3.2 Perovskite Oxyhydride

The common formula of the perovskite structure is ABO_3 and this is a fairly simple model that gives vast opportunities to combine different elements to achieve materials displaying different properties. The perovskite structure is also a very relevant oxide framework in relation to hydrogen dynamics, because of the extensive research on proton conducting perovskites.[15] Proton conducting perovskite oxides, such as $\text{BaTi}_{1-x}\text{Y}_x\text{O}_3\text{H}_x$ and $\text{BaCe}_{1-x}\text{Y}_x\text{O}_3\text{H}_x$, in which the protons (H^+) are covalently bound to oxygens of the perovskite host lattice, are currently accumulating considerable attention due to their promise as efficient electrolytes in a range of useful applications, such as fuel cells, hydrogen sensors, and electrochromic displays.[47, 48] The proton conduction mechanism is generally believed to be divided into two principal processes, hydrogen-bond mediated proton transfers (jumps) between neighbouring oxygen ions, and -OH reorientational motion between such transfers.[49] However, the local chemistry and structure, symmetry reduction, hydrogen-bonding interactions and proton-defect interactions *etc.*, complicate the description about proton dynamics that is still not fully understood for even the simplest systems.

A novel possibility to advance the understanding of hydrogen dynamics in

perovskite materials is given by the recently discovered perovskite oxyhydrides $ATiO_{3-x}H_x$ ($A = \text{Ba, Sr, Ca}$, $x < 0.6$).[50] In oxyhydrides, the hydrogen is of hydridic nature (H^-) and only a handful of other oxyhydrides have been reported so far, LaHO [51], $\text{Zr}_5\text{Al}_3\text{O}_{0.5}\text{H}_{4.8}$ [52], $\text{Ba}_{21}\text{Ge}_2\text{O}_5\text{H}_{24}$ [53], $\text{Ba}_3\text{AlO}_4\text{H}$ [54], $\text{Sr}_3\text{Co}_2\text{O}_{4.33}\text{H}_{0.84}$ [55], $12\text{CaO}\cdot 7\text{Al}_2\text{O}_3\cdot \text{H}$ [56] and $\text{LaSrCoO}_3\text{H}_{0.7}$ [57]. The hydride-ions in $ATiO_{3-x}H_x$ take the place of oxygen vacancies rather than being covalently bound to the oxygens as for the proton conductors. In contrast with most other oxyhydrides the systems $ATiO_{3-x}H_x$ are stable in air all the way up to *ca.* 400 °C, above which hydrogen is released. This observation leads to the conclusion that the hydride species in $ATiO_{3-x}H_x$ have to be mobile. This finding is highly exciting because it implies that the perovskite structural framework can accommodate both, cation (proton) and anion (hydride) conduction. In particular, interesting diffusion mechanisms specific to hydride-ions may exist in this material. The O^{2-} and H^- ions form the octahedral environment around Ti in this structure, which makes the Ti atoms exist in a mixed IV/III oxidation state.[50] This change of oxidation state makes the structure bigger as it has to accommodate another electron, which will make the material cubic at all temperatures (Fig. 3.2).[58] Compared to $ATiO_{3-x}H_x$, the pure BaTiO_3 instead goes through several structural changes, from a rhombohedral structure at low temperatures, through an orthorhombic structure at 183 K, to a tetragonal structure at 278 K and then to a cubic structure at temperatures above 396 K.[58] Notably, the presence of this extra electron in $ATiO_{3-x}H_x$ changes the color of the material from white to blue. The cause of the color change has been investigated by Schrader *et al.*[59], who suggested it to be due to the absorption of a specific wavelength that is attributed to a hopping process of small polarons. Polarons refer to electrons localized at specific sites, in this case on the Ti atom, rather than being delocalized within an electronic band.[60] However, there is still some controversy if the electron in $\text{BTiO}_{3-x}\text{H}_x$ creates a polaron or is located within the conduction band, so this needs to be investigated. Furthermore, the dynamics of hydride-ions are, as mentioned, not known. It has been hypothesized that when x is low, the migration of hydride-ions depends on the movement of oxide-ions, which is featured by a quite high activation energy (~ 0.8 eV), whereas when x is high, the concentration of hydride-ions is so high that the hydrogens may form a conduction

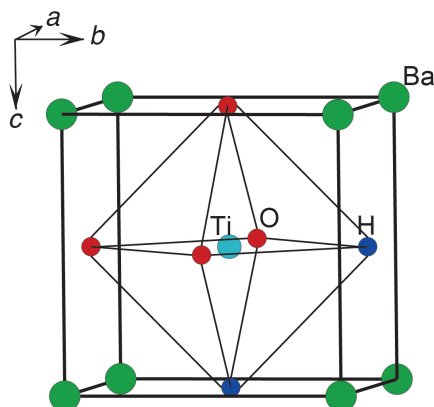


Figure 3.2: Schematic figure of the cubic-structured perovskite oxyhydride, $\text{BaTiO}_{3-x}\text{H}_x$.

pathway not dependent on the movement of oxygen ions.[50] If this is the case, the question is if there is an optimum hydride-ion concentration? Such information will provide new input into hydrogen dynamics in perovskite materials generally – now stretching from protic to hydridic species.

On the basis of the background given, this Thesis focuses on studies of the perovskite type oxyhydrides $\text{BaTiO}_{3-x}\text{H}_x$ ($x = 0.14$ and 0.40), in an attempt to determine both the position(s) and dynamical behavior of the hydride-ions. The aim is to investigate both the temperature and hydride-ion concentration dependence on the dynamics of the hydride-ions, as well as to compare with the properties of other related families of oxyhydrides and proton conducting oxides.[49] Example of other oxyhydrides of relevance include $\text{Ba}_3\text{AlO}_4\text{H}$, which exists as an inverse perovskite structure, X_3AB ($X = \text{Ba}^{2+}$ $A = \text{AlO}_4^{5-}$ and $B = \text{D}^-/\text{H}^-$). However, the structure is distorted due to the fact that the AlO_4^{5-} tetrahedron, as the A anion, is not spherical as it would be if it instead only consisted of an atom. The hydride-ion is bonded inside a strongly distorted Ba octahedron (HBa_6), where eight, corner-sharing HBa_6 octahedra units, will form a large three-dimensional framework. This three-dimensional framework creates a large void, filled by the AlO_4^{5-} units. This is a large and somewhat distorted structure compared to the much more simple perovskite structure of $\text{ATiO}_{3-x}\text{H}_x$. The structure of $\text{Ba}_3\text{AlO}_4\text{H}$ makes it difficult to predict the diffusional behavior of hydride ions. The more simple structure of $\text{ATiO}_{3-x}\text{H}_x$ makes it a better template (model system) for studies of hydride diffusion

mechanisms in oxyhydrides. Nonetheless, a comparison to $\text{Ba}_3\text{AlO}_4\text{H}$ and other structure types will provide important information on the influence of structure on the diffusional behavior of hydride-ions in an oxyhydride.[54]

Another interesting, relevant, oxyhydride, also exhibiting a special behavior of the extra electron, is C12A7:H ($12\text{CaO}\cdot 7\text{Al}_2\text{O}_3\cdot \text{H}$). The hydride ions in C12A7:H are not included in the lattice, but are captured in positively charged cages.[56] In the report by Hayashi *et al.* [56] the material is irradiated with ultraviolet light making the material to change from an insulator to an electronic conductor. A possible mechanism for the change to an electronic conductor is that the irradiated hydride-ions (H^-) split into H^0 and e^- . The electrically charged e^- will then leave and occupy another cage, where it will stay loosely bonded. Because it is only loosely bonded to the cage the wave function would then spread spatially and the electron may then migrate throughout the crystal by variable-range hopping. When heating the material to above 320°C , the light-induced conduction decreases and disappears. The hypothesis is that the H^0 atoms recombine and form H_2 molecules trapped inside the cages.[56] However, in the case of $\text{BTiO}_{3-x}\text{H}_x$, vibrational spectra may provide the answers of the behavior and positions of the extra electron. This could then be compared to the properties of C12A7:H.

Yet another oxyhydride of high relevance is $\text{LaSrCoO}_3\text{H}_{0.7}$. [61] This material is similar to $\text{ATiO}_{3-x}\text{H}_x$ as the hydride species in both materials replace some of the oxide anions in their role of linking the metal cations. Specifically in $\text{LaSrCoO}_3\text{H}_{0.7}$, the hydride-ions are located in the layers of CaO and are covalently bonded to Ca . [57] Interestingly, Bridges *et al.* [61] detected a long-range jump diffusion for the hydride-ions in $\text{LaSrCoO}_3\text{H}_{0.7}$. The hydride-ion hopping mechanism was found to initiate in the temperature range used for synthesis of the material and occurs in conjunction with loss of hydrogen from the sample. The resulted jump distance fitted well with that of the structure and gave approximately the distance between hydrogens, and the obtained activation energy and hydride-ion diffusion coefficient were *ca.* 200–230 meV and 6×10^{-5} – 10×10^{-5} cm^2s^{-1} in the temperature range of 700–750 K. [61] For comparison, these values are similar to what have been found for proton conducting oxide equivalents, *ca.* 400 meV and 1×10^{-6} cm^2s^{-1} . [49] The main tool for the dynamical investigation on $\text{LaSrCoO}_3\text{H}_{0.7}$ involved the use of quasielastic neu-

tron scattering, which is also the main technique used in this Thesis. Further technologies that have been used are inelastic neutron scattering and neutron diffraction. A brief description about these techniques, as well as about the particular instruments that have been used, is given in the following two chapters.

4

Neutron scattering techniques

Neutrons are electrically neutral and can therefore penetrate deep into solid materials. However, the cross section for hydrogens by neutrons is considerable large and therefore makes neutrons a most suitable tool, compared to other techniques, to observe hydrogen in solids.[62] The obtained quantity in neutron scattering experiments is the "scattering function", which describes how incident neutrons are scattered on a material (further explained in section 4.2 and 4.3). There are different characteristics of the scattering function, relating to coherent, incoherent, and elastic and inelastic scattering, see Fig. 4.1.[19]

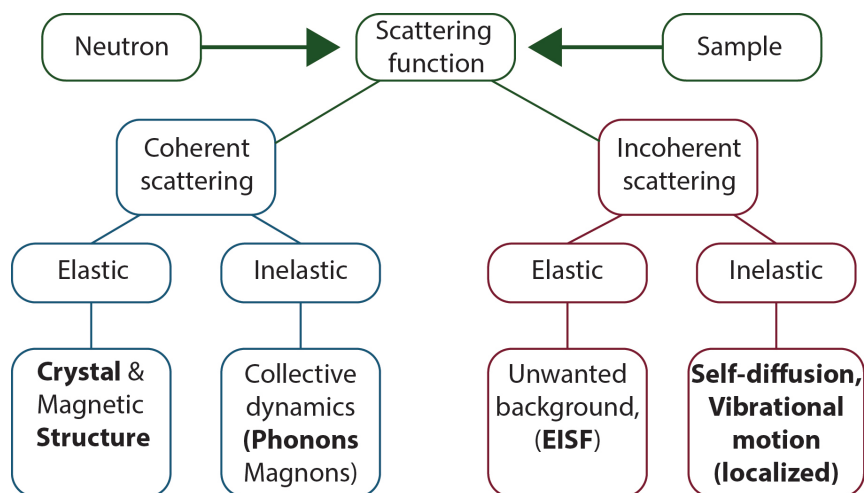


Figure 4.1: The scattering function, obtained from neutron scattering experiments and the different characteristics of this function together with the information that can be gained from the different parts of it.

The coherent part gives information about the atoms in relation to each other, thus providing information about crystal structure and collective dynamics. The incoherent part gives information about individual atoms, thus providing information about self-dynamics. In both these cases, the interaction with the material can be an elastic or an inelastic event, which means that the neutrons can either interact without any change of energy or lose/gain energy, respectively. The bold text in Fig. 4.1 are the characteristics and the corresponding experimental techniques that will be discussed in this Thesis.

4.1 Neutron diffraction

Even though neutron diffraction is in many ways similar to X-ray diffraction there is a big difference. The X-ray beam will primarily interact with the electron cloud in the studied material, whereas neutrons interact with the atomic nuclei. This will give a most interesting contrast to the measured diffraction pattern where it is often possible to distinguish between different isotopes of the same material but more importantly, makes it possible to detect hydrogen atoms.

For an elastic scattering event (Fig. 4.2) the following applies

$$k = |\mathbf{k}| = |\mathbf{k}'| = k' = \frac{2\pi}{\lambda}, \quad (4.1)$$

where k and k' is the wave number of the incident and the scattered wave, respectively. Because there is no change of energy between k and k' , the wave number is therefore preserved and hence the wavelength will not change.[63] Furthermore, the scattering vector, \mathbf{Q} , is then defined as

$$\mathbf{Q} = \mathbf{k}' - \mathbf{k}, \quad (4.2)$$

and the units for all the above are \AA^{-1} or reciprocal Ångström as it is usually called. The momentum lost from the neutron at collision is the momentum transfer, $\hbar\mathbf{Q}$, which comes from the particle-wave dualism defined by de Broglie, where the momentum of the particle corresponding to the wave with wave vector \mathbf{k} is given by $\mathbf{p} = \hbar\mathbf{k}$. Using trigonometry, the magnitude of \mathbf{Q} can be

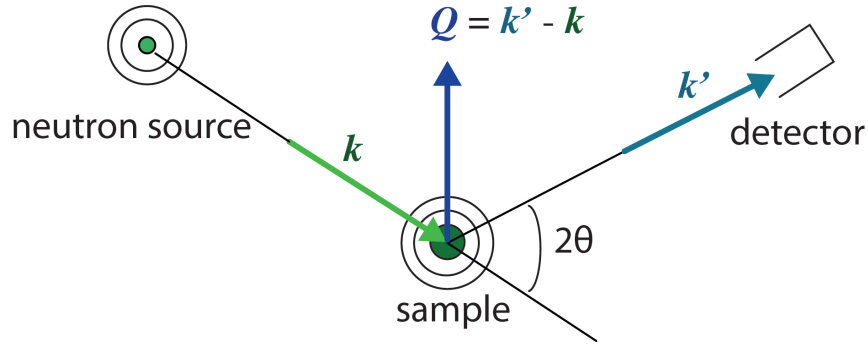


Figure 4.2: Schematic drawing of an elastic scattering process with the incoming wave with wavevector \mathbf{k} , the scattered wave with wavevector \mathbf{k}' and the scattering process with the sample by the scattering vector \mathbf{Q} .

written

$$|\mathbf{Q}| = Q = \sqrt{k^2 + k'^2 - 2kk' \cos 2\theta} \Rightarrow Q = \frac{4\pi}{\lambda} \sin \theta. \quad (4.3)$$

The measured quantity in a diffraction experiment is the intensity distribution as a function of the scattering vector $I(\mathbf{Q})$ and the intensity is then proportional to the cross section and the magnitude of Q related to the neutron wavelength and scattering angle according to Eq. 4.2.[19]

In this thesis, the structure of the oxyhydride, $\text{BaTiO}_{3-x}\text{H}_x$, was investigated using neutron diffraction, together with Rietveld analysis (full profile fitting) of the diffraction data.[64] The Rietveld method uses a least-square refinement technique in order to fit the observed diffraction pattern with a computer generated profile of an assumed structure. The aim of the investigation was to elucidate how the structure depends on x and also how the structure might change with temperature. Preliminary results are shown in Fig. 4.3. A key result is the well defined cubic structure for $x = 0.6$ [Fig. 4.3(a)]. However, for $x < 0.1$, the structure goes from cubic to slightly tetragonal [Fig. 4.3(b)]. This is consistent with previous reported first-principles calculations by Iwazaki *et al.*[58], who observed an increase of the structural volume when doping BaTiO_3 with a carrier electron. The increase of volume caused the structure to change from tetragonal to cubic. A reported threshold value was one electron in every tenth unit cell, which would correspond to an $x = 0.1$ for the oxyhydride, $\text{BaTiO}_{3-x}\text{H}_x$ structure.[58]

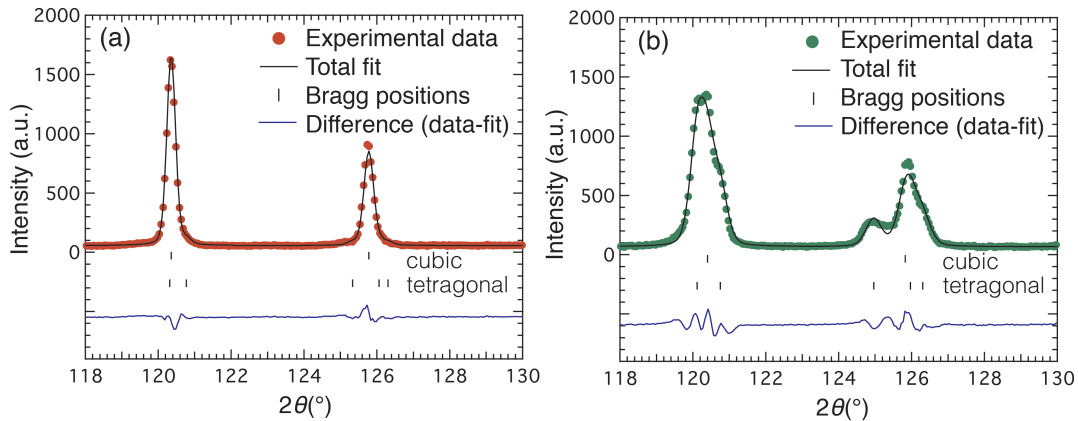


Figure 4.3: Diffraction pattern of (a) $\text{BaTiO}_{3-x}\text{D}_x$ ($x = 0.6$) and (b) $\text{BaTiO}_{3-x}\text{D}_x$ ($x = 0.07$), both are fitted with a tetragonal and a cubic structure. $\text{BaTiO}_{3-x}\text{D}_x$ ($x = 0.6$) shows a majority of a cubic phase (9% tetragonal and 91% cubic), whereas $\text{BaTiO}_{3-x}\text{D}_x$ ($x = 0.07$) shows a majority of tetragonal phase (64% tetragonal and 36% cubic).

4.2 Inelastic neutron scattering

Inelastic neutron scattering (INS) gives the opportunity to not only study the structure of the material but also the dynamics, a feature which is shared with inelastic X-ray scattering and dynamic light scattering, but with the difference that INS accesses exclusively the intermediate range of time (~ 0.5 ps to $1\mu\text{s}$) and space (~ 0.5 to 800 nm) where many of the interesting dynamical processes in materials are taking place. And, of course, INS also gives the unique opportunity to study hydrogens, which in the case of X-ray scattering are invisible.[19, 65]

The discussion in the previous section assumed that the neutron, at collision, preserved its energy, however, with INS the neutron can either preserve, gain or lose energy when interacting with the atoms of the material, which is depicted in Fig. 4.4. Now, because $k \neq k'$, Eq. 4.3 will therefore change to,

$$Q = \sqrt{k^2 + k'^2 - 2kk' \cos 2\theta} = \sqrt{\frac{8\pi^2}{\lambda^2} + \frac{2m\omega}{\hbar} - \frac{4\pi}{\lambda} \sqrt{\frac{4\pi^2}{\lambda^2} + \frac{2m\omega}{\hbar}} \cos 2\theta}. \quad (4.4)$$

In this new equation, Q is dependent on the energy, $\hbar\omega$, hence Q is no longer

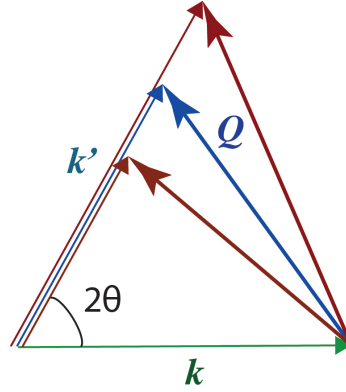


Figure 4.4: The difference in scattering vector, \mathbf{Q} , depending on if the scattering is elastic (blue) or inelastic (red), that is the neutron gains (big triangle) or loses energy (small triangle). The scattering vector is the resulting difference between the incident and the final wave vector, \mathbf{k} and \mathbf{k}' , respectively.

constant for a single scattering angle. Although, in the scattering process the energy and momentum are conserved. So the energy and momentum exchange are expressed as $\hbar\omega = E' - E$ and $\mathbf{Q} = \mathbf{k}' - \mathbf{k}$, respectively. Here, E is the incident energy of the neutron and \mathbf{k} is the incident wave vector, whereas E' and \mathbf{k}' are the energy and wave vector of the scattered neutron.

When using INS, one of the most important features investigated are the phonons in the crystal. Phonons are the vibrations of the lattice and can be treated as quasiparticles with a specific energy. Hence the scattering process can be viewed as a collision between phonons and neutrons, which will result in specific energy excitations.

An important aspect to discuss is how the phonons effect the elastic scattering, which is described by the Debye-Waller factor. This factor can be explained with a 'hand-waving' argument: atoms are displaced by a vector u_j from their nominal lattice position due to the thermal vibrations. The value of $\langle u \rangle$ is on average zero, but there will be a finite mean-square displacement $\langle u^2 \rangle$. The Debye-Waller factor can be shown to be [19]

$$\exp(-\langle (\mathbf{Q} \cdot \mathbf{u}) \rangle) = \exp(-Q^2 \langle u^2 \rangle / 3). \quad (4.5)$$

Important to note is that the second expression is only valid for isotropic conditions. The result of this is that the elastic peaks get less defined with increasing

temperature and also with increasing Q . [19]

The mean-square displacement (MSD) can be calculated from measurements of elastic fixed window scans (FWSs), *i.e.* measurements of the elastic intensity as a function of temperature. MSD generally shows a linear behavior at low temperatures and as the vibrations of the material get activated at higher temperatures, the slope of the MSD will change.

Vibrations involve interaction in the entire lattice of the material, therefore the part of the scattering function, $S(Q, \omega)$, that is of interest is the coherent part, $S_{\text{coh}}(Q, \omega)$. It can be shown that the intensity of the i th molecular vibrational transition, is then proportional to:

$$S_{\text{coh}}(Q, \omega_i) \propto I_i \propto Q^2 U_i^2 \exp(-Q^2 u_{\text{Total}}^2) \sigma, \quad (4.6)$$

where ω_i is the i th mode at frequency ω and U_i is the amplitude of vibration of the atom undergoing the particular mode. [66] The exponential term is again the Debye-waller factor, with u_{Total} as the mean-square displacement of all the atoms in all the modes, both internal and external, and σ is the inelastic cross section of all the atoms involved in the mode. Hence, if there is no translational diffusion, the intensity decays as [25]

$$I(Q) \approx e^{-Q^2 \langle u^2 \rangle / 3}, \quad (4.7)$$

where $\langle u^2 \rangle$ is the MSD. The change of slope of the MSD that depends on the vibrations in the material can be calculated from the INS spectra of the material. Any deviation from this when increasing temperature gives information about the temperature range that the anharmonic vibrational or diffusional motions in the material will become accessible for the instrument.

4.3 Quasielastic neutron scattering

For diffusional motion studies, the main part to investigate of the scattering function, $S(Q, \omega)$ is the incoherent part. Furthermore, as previously mentioned, the interest of this Thesis is investigating the self-dynamics of hydrogen, which have a large incoherent cross section and a smaller coherent one. In effect,

the total dynamical structure factor can be approximated with the incoherent dynamical structure factor, *i.e.* $S(Q, \omega) \approx S_{\text{inc}}(Q, \omega)$.

For low-energy neutrons (0.05-100 meV), there will be an interaction between the neutrons and the hydrogens resulting in an energy gain or energy loss of the kinetic energy of the neutrons, not unlike the INS. However, INS relates to periodic dynamics with specific frequencies/energies, whilst QENS refers to stochastic motions which are centered around the elastic peak (corresponding to the zero energy loss/gain neutrons) and observed as a broadening of the previous mentioned (Fig. 4.5).[21, 22] Furthermore, the time scales for diffusional dynamics are usually longer than for vibrational dynamics resulting from INS.

The two most important features of the QENS peak, where the main information can be gained, is the area $[A_i(Q)]$ and the full width at half maximum $[\Gamma_i(Q)]$ and how they both change with Q . In order to extract this information of the dynamics in the system, the measured structure factor, $S_{\text{meas}}(Q, \omega)$ can be modeled with

$$S_{\text{meas}}(Q, \omega) = S_{\text{inc}}(Q, \omega) \otimes R(Q, \omega), \quad (4.8)$$

where Q is the momentum transfer and ω is the frequency.[34] The instrumental resolution is represented by $R(Q, \omega)$ in the above equation. Often, there will also be a background in the measured spectra corresponding to peak tails of fast atomic vibrations (INS). In the case of (pure) quasielastic scattering, $S_{\text{inc}}(Q, \omega)$ may be expressed as

$$S_{\text{inc}}(Q, \omega) = A_0(Q)\delta(\omega) + \sum_i A_i(Q)L_i(Q, \omega), \quad (4.9)$$

where the elastic peak is represented with a delta function, $\delta(Q, \omega)$ and where the $L_i(Q, \omega)$ s are Lorentzian functions describing the quasielastic peak of the form

$$L_i(Q, \omega) = \frac{2}{\pi} \frac{\Gamma_i(Q)}{(2\hbar\omega)^2 + \Gamma_i(Q)^2}. \quad (4.10)$$

$\hbar\omega$ is the neutron energy transfer and $\Gamma_i(Q)$ is the Lorentzian's full width at half maximum. $\Gamma_i(Q)$ relates to a characteristic relaxation, also known as correlation, time, τ_i , of the dynamics giving rise to quasielastic scattering,

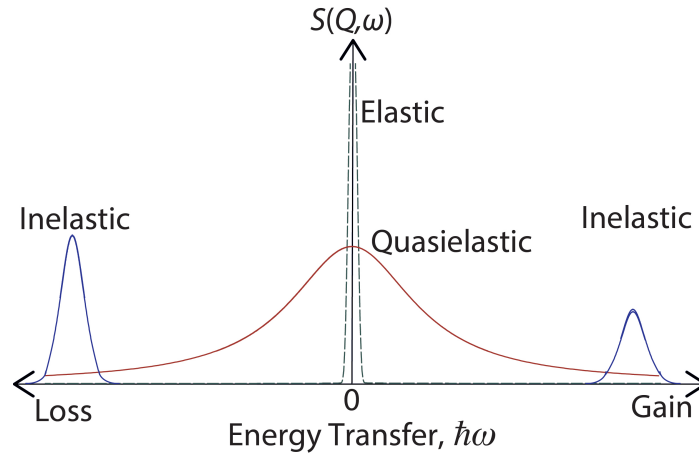


Figure 4.5: $S(Q, \omega)$ of a fixed Q -value, with a quasielastic peak, the elastic peak and the inelastic peaks further out from the zero energy transfer point ($\hbar\omega=0$).

according to

$$\tau_i = \frac{2\hbar}{\Gamma_i}. \quad (4.11)$$

Hence, the Lorentzian functions, through $\Gamma_i(Q)$ and $A_i(Q)$, contain information about both the time-scale and Q -dependence of the observed dynamics. Additionally, the area, A_0 and A_i , of the QENS peak over Q can give information about the spatial characteristics of the dynamics.

Since the QENS spectra are measured as a function of Q , the geometry of the observed localized motion(s) can be obtained from the ratio of the elastic (incoherent) scattering intensity $A_0(Q)$, [Eq. (4.9)] to the total (incoherent) scattering intensity, plotted as a function of Q . The total incoherent scattering intensity is the sum of the intensities of the elastic and quasielastic scattering and follows the assumption that the quasielastic and vibrational motions are separable, *i.e.* they occur on different time-scales. The resulting function is commonly referred to the elastic incoherent structure factor (EISF),

$$\text{EISF} = \frac{A_0(Q)}{A_0(Q) + A_i(Q)}, \quad (4.12)$$

where $A_i(Q)$ is the area of the Lorentzian describing the quasielastic peak.[32] The EISF is unity at $Q = 0$ and falls to a minimum at a Q -value that, importantly, relates to the spatial geometry of the dynamics. For instance, for a

jump motion between three equivalent sites, the EISF is an oscillatory function of Q that approaches $1/3$ at large values of Q , whereas a jump motion between four equivalent sites yields a different oscillatory EISF function that approaches $1/4$ at large values of Q . [67] Therefore, higher- Q data are often needed to distinguish between likely models in order to include this critical minimum. This requires using higher-energy (shorter-wavelength) neutrons, but necessarily results in poorer energy resolution, which is a largely unavoidable characteristic of neutron spectrometers. By comparing the experimental EISF with geometrically feasible models, the geometry of motion can often be revealed. A general expression for the EISF (A_0) can be generated for N number of equivalent sites according to

$$A_0(Q) = \frac{1}{N} \sum_{n=1}^N j_0(Qr_n), \quad (4.13)$$

where j_0 is the zeroth-order spherical Bessel function [$j_0 = \sin(x)/(x)$]. [21] By comparing the experiment EISF with physically sound theoretical models, the geometry of the observed motion can often be analyzed. The approach is to identify a likely model that would correspond to the structure of the material, following a process of fitting the model to the EISF over Q . Below follows the mathematical expression for the exploited EISF models as considered in this Thesis for hydrogen dynamics in $ASiH_3$ ($A = K$ and Rb).

Four different reasonable models for the reorientational motion of SiH_3^- ions can be imagined, namely (i) 120° reorientations of the SiH_3^- around the C_3 axis, (ii) free rotational motion around the C_3 axis, (iii) isotropic diffusional motion, and (iv) rotational diffusion around 24 sites. Fig. 4.6 show the EISFs corresponding to these models.

Considering first model (i), the structure of SiH_3^- [Fig. 3.1(b)], would suggest a model characterized by jumps between three equivalent sites (C_3 axis rotations), this because the molecule of SiH_3^- consists of three hydrogens bonded to the Si atom. Hence, for the model for C_3 axis rotations the EISF takes the form

(i) C_3 axis rotations:

$$EISF_{C_3} = \frac{1}{3} [1 + 2j_0(\sqrt{2}r_1Q)]. \quad (4.14)$$

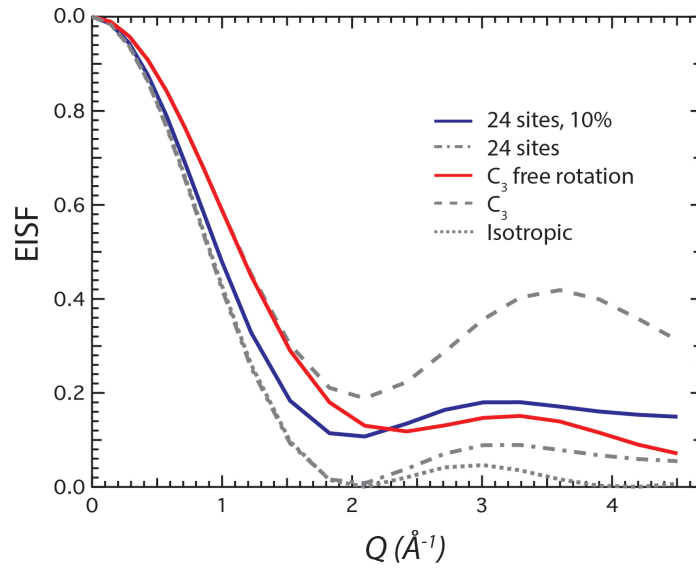


Figure 4.6: Models for the EISF, presenting five models, free rotation about the C_3 axis (red), 24 hydrogen sites situated around the Si atom with 10% of the hydrogen immobile (blue), 3-site jumps around the C_3 axis (dashed line), the dashed and dotted line is the same as the blue curve but with no immobile hydrogen and the isotropic rotational diffusion model where all positions around the Si atom is possible (dotted line).

Next, model (ii), the hydrogens performs free rotations around the C_3 axis (C_3 free rot.). A general formula is then easily realized where the angle changes with the number of sites[67]

(ii) *Free rotational diffusion around the C_3 axis:*

$$\text{EISF}_{\text{free rot.}} = \frac{1}{N} \sum_{n=1}^N j_0[2Qr \sin(\frac{n\pi}{N})], \quad (4.15)$$

When N increases, the curve will approach a specific shape and position. For $N \geq 50$, the rotational diffusion may be considered as free diffusion around a circle with radius r .

In model (iii) the minimum of the EISF should approach 0, and hence indicates the limiting case of isotropic rotational diffusion. The molecule is then free to reorient in any direction with small jump distances and the probability of the hydrogen positions is therefore anywhere on a sphere with the radius of r surrounding the center of mass atom.

(iii) *Isotropic rotational diffusion on a sphere:*

$$\text{EISF}_{\text{iso}} = j_0^2(Qr). \quad (4.16)$$

Model (iv) allows the hydrogen atoms to move between 24 different sites on a sphere surrounding the Si atom and can be structured from the isotropic rotational diffusion model. As the SiH_3^- molecule is confined inside a cubic lattice, a reasonable model would be to let the hydrogen move from corner to corner inside a cube. However, when considering the geometry of the molecule it is apparent that it would not fit perfectly in the corners, but the positions of the hydrogen would be distorted. For every corner position this would generate three hydrogen positions and therefore generate a total number of 24 positions on a sphere around the Si atom close to the corner of the cube [Fig. 3.1(a)]. Hence a model describing jump diffusion on the surface of a sphere with 24 different jump locations, corresponding to the H atom position in $\alpha\text{-ASiH}_3$ would be a reasonable description.

(iv) *Rotational diffusion on a sphere with 24 different jump locations:*

$$\text{EISF}_{24 \text{ sites}} = \frac{1}{24} [1 + j_0(Qd_1) + j_0(Qd_2) + \dots j_0(Qd_{23})], \quad (4.17)$$

where the 23 jump distances (d_1, d_2, \dots, d_{23}) correspond to the 24 different H locations of $\alpha\text{-ASiH}_3$, which have been determined on the basis of neutron diffraction data.[13] However, the EISF of $\alpha\text{-ASiH}_3$ did not fit to this model adequately, but showed a small offset. This had to be accounted for and therefore, 10% of immobile H atoms, as described in **Paper II**, was added to the model,[68]

$$\text{EISF}_{24 \text{ sites}, 10\% \text{ immobile H}} = 0.9 \times \text{EISF}_{24 \text{ sites}} + 0.1. \quad (4.18)$$

In Fig. 4.6 the model in blue represents model (iv) with this addition of 10% immobile hydrogen atoms. This model fitted extremely well to the data and was therefore accepted as the dynamical model describing the motion in both of the materials.

Neutron scattering techniques, presented in this Chapter, have been shown to be most useful to investigate hydrogens in materials. In order to perform

neutron scattering experiments, the proper instrumentation has to be used, suited for the time scale and hypothesis wished to be investigated. There is a vast number of facilities and instruments to choose from, but in the next chapter, a small collection of instruments associated with this Thesis will be presented.

5

Instrumentation

There are two main types of neutron sources, a spallation source, where the neutrons are generated by colliding accelerated charged particles into a heavy element (target), or a reactor, where neutrons are produced through fission. A key difference between the two is that with a spallation source the neutrons are produced in pulses as the particles hit the target material, whereas in a reactor source neutrons are continuously produced. In this thesis, I have used instruments on both reactor and spallation sources. The neutrons from both sources have a high velocity/energy when they are produced and therefore need to be slowed down by the help of moderators made of, for example, heavy water. This will give neutrons characterized by different ranges of energies/wavelengths utilized in the different techniques.[19]

The main disadvantage with using neutrons as a tool to extract the characteristics of a material is the low flux compared to other techniques, for example those based on X-rays. This is due to the low flux from the source itself. However, the beam generally needs to be monochromatized, hence the flux is reduced even further. As a consequence, measurements are generally long (of the order of days) and instruments are not readily available. In this thesis, I have used four different instruments, the two quasielastic spectrometers DCS and HFBS at the NIST Center for Neutron Research (NCNR), and the diffractometer D2B at ILL. A concise description about the key aspects of each instrument is given in the following.

5.1 The DCS quasielastic spectrometer

The time-of-flight disk chopper spectrometer (DCS)[69] at NCNR, Gaithersburg (USA), is a powerful instrument for the investigation of hydrogen dynamics in materials. It uses neutrons with wavelengths in the range ~ 2.3 to ~ 10 Å, which are selected by a monochromating chopper system.[70] The chopper system is based on a set of rotating discs, which are synchronized so that only neutrons with a specific wavelength (energy) passes through them and reach the instrument. This turns the beam into pulses which are then utilized during detection through the time-of flight technique. The determination of energy exchange during the scattering event is then based on the measurement of the time-of-flight before and after scattering. With the use of 2.5 Å neutrons, the energy resolution and accessible Q -range of the spectrometer are 745 μeV at full width at half maximum (FWHM), and 0.98–4.48 Å⁻¹, respectively. The accessible relaxation times are (hence) of the order ~ 0.01 ps to ~ 1 ps. If using a longer wavelength the energy resolution increases but the Q -range is reduced. The slowest dynamics that can be probed by DCS are characterized by time-scales of the order 100 ps. If even longer time-scale dynamics are of interest, a backscattering spectrometer, such as High Flux Backscattering Spectrometer (HFBS), may be used.

5.2 The HFBS quasielastic spectrometer

HFBS provides a good complement to the DCS instrument, as it has better resolution (0.83 μeV), thus allowing slower time scale dynamics to be observed (~ 0.01 -1 ns).[71] Further, HFBS allows the measurements of fixed window scans (FWSs), which are measurements of the elastic intensity as a function of temperature. The FWSs measurements are often very useful for determining the temperature at which the dynamics are accessible to the instrument.

The monochromization of the incoming neutron beam is achieved by Bragg-diffraction on a mono-crystal. In this context, the wavelength spread $\delta\lambda$, of a Bragg-diffracted neutron beam decreases as the scattering angle, 2θ , approaches 180°, according to[72]

$$\frac{\delta\lambda}{\lambda} = \frac{\delta d}{d} + \frac{\delta\theta}{\tan\theta}. \quad (5.1)$$

Hence, if the neutrons are scattered 180° (backscattering), that is θ approaches 90° , the term containing the angle vanishes. The only term then left to influence the wavelength divergence is the d -spacing term. Therefore by choosing a material for the monochromator with an appropriate spread in spacing can influence the beam convergence significantly. Silicon (111) plane is the one most commonly used, with a $\frac{\delta d}{d}$ of 1.86×10^{-5} . With this configuration the beam will become more monochromatic and give a better resolution.

5.3 The TOSCA inelastic spectrometer

TOSCA is an inelastic neutron spectrometer used for the determination of vibrational spectra of materials.[73, 74] It is the neutron counterpart to its optical analogues, Raman and infrared spectroscopy. A key difference between INS and optical spectroscopy is that INS is not subjected to any optical selection rules, so that all vibrations are in principle measurable. The reason for this is that INS is dependent on the neutron cross-section of the atoms and not from changes in the electronic properties of the molecule that occur as the vibration is excited, as in the case for Raman and infrared spectroscopy. TOSCA is situated at the ISIS pulsed spallation neutron source at the Rutherford Appleton Laboratory, Chilton, Didcot, Oxfordshire, UK and is more specifically an indirect geometry time-of-flight spectrometer. This means that the time-of-flight technique is used for energy analysis of the scattered neutrons, where the final energy is a known, fixed value, compared to the direct geometry instruments where the incident energy instead is fixed.[75]

For TOSCA there is only a sum of a range of Q values detected for each energy, whereas in other INS instruments there is the possibility to also obtain a Q -dependence. TOSCA covers the range from 0 to 8000 cm^{-1} of the vibrational spectrum in a single measurement and the samples under investigation may be mounted on a multi-sample-changer, allowing for the measuring of several samples without the need to take out the sample stick between each measurement. Both of these technical characteristics of TOSCA makes it an easy and user-friendly instrument. TOSCA also provides the possible to measure a diffraction pattern of the sample, although with low resolution. For a

more careful structural analysis a high-resolution diffractometer, such as D2B at the ILL, should be used.

5.4 The D2B diffractometer

The D2B diffractometer is a high resolution instrument, featured by a high take-off angle (135°) for the monochromator.[76] D2B is situated at the Institute Laue Langevin (ILL, Grenoble) and uses thermal neutrons to detect a diffraction pattern. There is a range of possible wavelengths to use on D2B. For example will $\lambda = 1.051 \text{ \AA}$ include more visible peaks, however the intensity will be lowered by a factor of 4 compared to $\lambda = 1.594 \text{ \AA}$ that in turn will show less diffraction peaks. There is also a wide range of possible sample environments that can be mounted with up to 5 different samples at the same time, which could include; three in room temperature and room pressure, one in the cryofurnace (1.5 to 525 K) and one in the furnace (200 to 1000 K) under vacuum. The great advantage of neutron diffraction, compared to X-ray diffraction, is the possibility to observe hydrogen atoms, thanks to hydrogens' large neutron scattering cross section. This gives the opportunity to determine the location of hydrogen atoms in the structure, as well as site occupancy and atomic displacement parameters etc., which is of great importance for the materials studied in this thesis.

6

Summary of appended papers

Paper I

The two alkali silanides $ASiH_3$ ($A = K$ and Rb) were investigated by means of quasielastic neutron scattering, both below and above the order-disorder phase transition temperature occurring at around 270–305 K. Measurements upon heating show the onset of strong quasielastic scattering around the phase-transition temperature demonstrating that the phase-transition is dynamical in nature. In order to describe the dynamics, the previously reported structure of a quasi-spherical arrangement with 24 sites of preferred orientations for the hydrogen atoms around each Si atom was used as a starting point in the analysis of the quasielastic data. In somewhat more detail, a reorientation model was considered, that do not necessarily preserve a particular orientation of the SiH_3^- ions in the NaCl-type crystal structure, but in fact describes a jump diffusion on the surface of a sphere, with 24 different jump locations. This model represents a combination of a rotational diffusion motion and a localized jump model. The model is similar to the isotropic rotational diffusion model, but with the difference that it includes small jump distances to preferred hydrogen sites. Additionally, to get a satisfactory and physically sound fit, a constant of 0.1 (10%) was added to the model, in order to account for scattering of H atoms that do not contribute to the observed dynamics. A suggested explanation for the missing 10% of quasielastic scattering was that there were some diffusional information lost in the background subtraction of the analysis, due to diffi-

culties to separate the background, probably arising from vibrational motions, from the very fast diffusional motion, originating from continuous rotational diffusion on a circle around the eight C_3 axes. The average relaxation time between successive jumps is of the order of sub-picoseconds and exhibits a weak temperature dependence with a small difference in activation energy between the two materials, 39(1) meV for KSiH_3 and 33(1) meV for RbSiH_3 . Besides being of considerable fundamental interest, the better understanding of the nature of SiH_3^- orientational mobility in the disordered phases of KSiH_3 and RbSiH_3 may explain the low entropy variation for hydrogen absorption/desorption and hence the origin of these materials' favorable hydrogen-storage properties.

Paper II

The perovskite type oxyhydrides $\text{BaTiO}_{3-x}\text{H}_x$ ($x = 0.14$ and 0.40) were investigated with inelastic and quasielastic neutron scattering, with the aim to determine the position(s) and dynamical behavior of the hydride-ions in these materials. The results show that the hydride-ions are located on vacant oxygen sites of the perovskite lattice, with the presence of Ti-H vibrational modes at 916(5) and 1037(5) cm^{-1} for $x = 0.14$, and at 911(5) and 1027(5) cm^{-1} for $x = 0.4$. No signature of O-H stretch modes were observed in the spectra, showing that the hydrogens are not covalently bonded to the oxygens, as in proton conducting equivalents such as $\text{BaTi}_{1-x}\text{Y}_x\text{O}_3\text{H}_x$. Measurements of the MSD suggest not only the presence of vibrational motions of H, but also the presence of diffusional H motion. The diffusional H dynamics were investigated with QENS at the temperatures 275, 375 425 and 500 K and revealed dynamics on the time-scale of the order of one nanosecond and with a very weak temperature dependence. The relatively long time-scale of the observed dynamics would suggest a long-range diffusional behavior, however the Q -dependence of the quasielastic width would, on the contrary, not support such a conclusion.

7

Conclusions and outlook

This Thesis has provided important information about the behavior of hydrogen in two classes of energy relevant materials, (i) alkali silanides and (ii) perovskite oxyhydrides. Paper I reports on the localized diffusional behavior of hydrogen atoms in $ASiH_3$ ($A=K, Rb$), showing a jump diffusion on the surface of a sphere with 24 different jump locations. Paper II reports on the vibrational motion of hydride-ions, confirming that the hydride-ions are located on vacant oxygen sites of the perovskite lattice, as suggested in the literature. In addition, the diffusional motion of hydride-ions is detected with quasielastic neutron scattering. Besides being of considerable fundamental interest, these results are also of importance from a technological point of view in view of the development of next-generation hydrogen-storage and fuel-cell materials. Also, the main tool of investigating hydrogens, neutron scattering, has been explained and the different techniques in relation to the specific related instruments. The great advantages with neutron scattering techniques have been highlighted and what unique and highly useful information that can be gained.

Looking into the future, there are lots of possibilities to extend the presented studies. Concrete sequels to the results of this thesis will include

- ▷ the investigations of SiH_3^- dynamics in the low temperature phase, an extended study of $ASiH_3$ ($A = K, Rb$) at temperatures below 270-305 K, and also to include $CsSiH_3$ in this study. The aim is to elucidate how the phase transition of the material influences the dynamics and also to get a further understanding of the influence of the A atom.

- ▷ the investigations of localized and long-range diffusion of H^- atoms in $\text{ATiO}_{3-x}\text{H}_x$ and how it depend on A ($A = \text{Ca}, \text{Sr}$ and Ba), temperature and on x . The aim is to elucidate how the A site ion influences the diffusional path and vibrational frequencies in order to learn even more about the diffusional nature of H^- in perovskite oxyhydrides.
- ▷ the investigations of the dynamical behavior and conduction of hydride-ions in $\text{BaTiO}_{3-x}\text{H}_x$ synthesized as a film and how this depends on x . The purpose is to investigate the hydride-ion dynamics in a material more similar to the electrolyte material in a fuel cell. This will enable conduction studies together with the effect of of strain in the material and how it influences the diffusion of hydride-ions.
- ▷ the investigations on the highly reduced structure and vibrational behavior of BaTiO_{3-x} , as this material was successfully synthesized during a previous diffraction experiment. A study of this material would be of high relevance to the research program as it provides complementary knowledge of the influence of the hydride-ion in $\text{BaTiO}_{3-x}\text{H}_x$.
- ▷ the investigations of the optical vibrational spectra of $\text{BaTiO}_{3-x}\text{H}_x$ with the aim to complement the INS spectra and hence to learn more about the local structure of perovskite oxyhydrides.
- ▷ and the investigations of the computational vibrational spectrum compared to the experimentally measured inelastic spectrum together with the optical vibrational spectrum of $\text{BaTiO}_{3-x}\text{H}_x$. A specific aim is to verify the role of the extra electron (as a polaron or distributed in the conduction band) and also to obtain more detailed knowledge about how the H^- influences the lattice vibrations.

As a final note, an indirect goal of my PhD is to learn about neutron techniques in order to increase the competence within this field in Sweden. The future of neutrons is to be used as a material analyzing tool in Sweden, and will become of great importance as the completion of the European Spallation Source, ESS, situated in Lund, Sweden, is getting closer.[77]

Acknowledgements

I would like to thank my main supervisor Maths for his readiness and support with this thesis, the fast comments and for giving me the opportunity to do my PhD at Chalmers. Thanks to my office mates, Martin and Andrea, for moral support and discussions, both scientific and nerdy. Thanks to my colleagues Laura, Daria and Yuan-Chih, for helping with my projects and also for your vital friendship. Thanks to Ezio for his support in the lab, my co-supervisor Göran for the inspiring discussions, Ulrich group in Stockholm for synthesizing the materials and to all my other colleagues at CMP for the great support and all the super interesting lunch discussions.

Finally, I would like to thank my parents Marie and Thomas and also my brother Eric. And a special thank to Johnas, my best friend and loving husband.

Carin

Bibliography

- [1] H. Liu, A. Almansoori, M. Fowler and A. Elkamel, *International Journal of Hydrogen Energy*, 2012, **37**, 8905–8916.
- [2] J. Ren, S. Gao, S. Tan, L. Dong, A. Scipioni and A. Mazzi, *Renewable and Sustainable Energy Reviews*, 2015, **41**, 1217–1229.
- [3] M. Stygar and T. Brylewski, *International Journal of Hydrogen Energy*, 2013, **38**, 1–9.
- [4] M. Pudukudy, Z. Yaakob, M. Mohammad, B. Narayanan and K. Sopian, *Renewable and Sustainable Energy Reviews*, 2014, **30**, 743–757.
- [5] H. Wang, H.-W. Lee, Y. Deng, Z. Lu, P.-C. Hsu, Y. Liu, D. Lin and Y. Cui, *Nat Commun*, 2015, **6**, 1–8.
- [6] M. Navarro, *H2OCEAN development of a wind-wave power open-sea platform equipped for hydrogen generation with support for multiple users of energy*, <http://www.h2ocean-project.eu/>, accessed 2016-04-19.
- [7] C. Benjaminsen, *Fishing vessel transformed into a wave power plant*, <http://sciencenordic.com/fishing-vessel-transformed-wave-power-plant>, accessed 2016-04-19.
- [8] *FCV Fuel Cell Vehicle*, <http://www.toyota-global.com/innovation/>, accessed 2016-04-19.
- [9] N. de Miguel, R. O. Cebolla, B. Acosta, P. Moretto, F. Harskamp and C. Bonato, *International Journal of Hydrogen Energy*, 2015, **40**, 6449 – 6458.

- [10] R. Hirotsu, T. Terada, Y. Tamura, H. Mitsuishi and S. Watanabe, *Thermal Behavior in Hydrogen Storage Tank for Fuel Cell Vehicle on Fast Filling.*, Society of Automotive Engineers Technical Report 2007-01-0688, 2007.
- [11] J.-N. Chotard, W. S. Tang, P. Raybaud and R. Janot, *Chem. Eur. J.*, 2011, **17**, 12302–12309.
- [12] W. Tang, J. Chotard, P. Raybaud and R. Janot, *J. Phys. Chem. C*, 2014, **118**, 3409–3419.
- [13] V. F. Kranak, Y.-C. Lin, M. Karlsson, J. Mink, S. T. Norberg and U. Häussermann, *Inorg. Chem.*, 2015, **54**, 2300–2309.
- [14] O. L. C. Sylwan, *Nationalencyklopedin, bränslecell.*, <http://www.ne.se/uppslagsverk/encyklopedi/lång/bränslecell>, accessed 2016-04-19.
- [15] K. D. Kreuer, *Annu. Rev. Mater. Res.*, 2003, **33**, 333–359.
- [16] F. A. de Bruijn, V. A. T. Dam and G. J. M. Janssen, *Fuel cells 08*, 2008, **1**, 3–22.
- [17] D. E. Lehmann, *Neutron Imaging for Cultural Heritage Investigations*, <https://www.psi.ch/niag/cultural-heritage>, accessed 2016-04-21.
- [18] N. B. Colthup, L. Daly and S. Wiberley, *Introduction to Infrared and Raman Spectroscopy*, Academic Press: London, Third Edition edn., 1964.
- [19] T. Brückel, J. Voigt, G. Heger, G. Roth, H. Frielinghaus, J. Stellbrink, R. P. Hermann, E. Kentzinger, U. Rücker, R. Zorn, M. Angst and D. Richter, *Neutron scattering*, Forschungszentrum Jülich GmbH, 2014, vol. 84.
- [20] O. Beckman, *Nationalencyklopedin, fonon.*, <http://www.ne.se/uppslagsverk/encyklopedi/lång/fonon>, accessed 2016-04-21.
- [21] M. Bée, *Quasielastic Neutron Scattering*, IOP Publishing, Bristol, D.J. Millen ed., 1988.

- [22] R. Hempelmann, *Quasielastic neutron scattering and solid state diffusion*, Clarendon Press, Oxford, 2000.
- [23] J. Crank, *The mathematics of diffusion*, The Clarendon Press, Oxford., 1956.
- [24] . Truls Norby, University of Oslo, *Chapter 5, Diffusion*, <http://www.uio.no/studier/emner/matnat/kjemi/KJM5120/h10/undervisningsmateriale/KJM5120-Defects-and-transport-compendium-Ch5-2010.pdf>, accessed 2016-04-12.
- [25] K. J. Alvine, M. Tyagi, C. M. Brown, T. J. Udovic, T. Jenkins and S. G. Pitman, *J. Appl. Phys.*, 2012, **111**, 053505–1 – 053505–7.
- [26] L. Schlapbach and A. Züttel, *Nature*, 2001, **414**, 353–358.
- [27] U. Eberle, M. Felderhoff and F. Schüth, *Angew. Chem.*, 2009, **48**, 6608–6630.
- [28] P. Chen, Z. Xiong, J. Luo, J. Lin and K. L. Tan, *Nature*, 2002, **420**, 302–304.
- [29] P. Chen, Z. Xiong, J. Luo, J. Lin and K. L. Tan, *J. Phys. Chem. B*, 2003, **107**, 10967–10970.
- [30] A. Züttel, S. Rentsch, P. Fischer, P. Wenger, P. Sudan, P. Mauron and C. Emmenegger, *J. Alloys Compd.*, 2003, **356-357**, 515–520.
- [31] A. Züttel, A. Borgschulte and S. Orimo, *Scr. Mater.*, 2007, **56**, 823–828.
- [32] N. Verdál, M. R. Hartman, T. Jenkins, D. DeVries, J. J. Rush and T. J. Udovic, *J. Phys. Chem. C*, 2010, **114**, 10027–10033.
- [33] N. Verdál, T. J. Udovic and J. J. Rush, *J. Phys. Chem. C*, 2012, **116**, 1614–1618.
- [34] N. Verdál, T. J. Udovic, J. J. Rush, H. Wu and A. V. Skripov, *J. Phys. Chem. C*, 2013, **117**, 12010–12018.
- [35] N. Verdál, T. J. Udovic, J. J. Rush, X. Liu, E. H. Majzoub, J. J. Vajo and A. F. Gross, *J. Phys. Chem. C*, 2013, **117**, 17983–17995.

- [36] B. Bogdanovic and M. Schwickardi, *J. Alloys Compd.*, 1997, **253-254**, 1–9.
- [37] B. Bogdanovic, R. A. Brand, A. Marjanovic, M. Schwickardi and J. Tolle, *J. Alloys Compd.*, 2000, **302**, 36–58.
- [38] Z. Xiong, C. K. Yong, G. Wu, P. Chen, W. Shaw, A. Karkamkar, T. Autrey, M. O. Jones, S. R. Johnson, P. P. Edwards and W. I. F. David, *Nat. Mater.*, 2008, **7**, 138–141.
- [39] N. Verdal, T. J. Udovic, J. J. Rush, V. Stavila, H. Wu, W. Zhou and T. Jenkins, *J. Chem. Phys.*, 2011, **135**, 094501–1 – 094501–8.
- [40] H. Wu, W. Zhou, F. E. Pinkerton, T. J. Udovic, T. Yildirim and J. J. Rush, *Energy Environ. Sci.*, 2012, **5**, 7531–7535.
- [41] M. A. Ring and D. M. Ritter, *J. Am. Chem. Soc.*, 1961, **83**, 802–805.
- [42] E. Weiss, G. Hencken and H. Kuhr, *Chem. Ber.*, 1970, **103**, 2868–2872.
- [43] O. Mundt, G. Becker, H.-M. Hartmann and W. Z. Schwarz, *Anorg. Allg. Chem.*, 1989, **572**, 75–88.
- [44] C. Österberg, H. Fahlquist, U. Häussermann, C. M. Brown, T. J. Udovic and M. Karlsson, *The Journal of Physical Chemistry C*, 2016, **120**, 6369–6376.
- [45] R. D. Shannon, *Acta Cryst. A*, 1976, **32**, 751–753.
- [46] P. Martelli, A. Remhof, A. Borgschulte, R. Ackermann, T. Strässle, J. Embs, M. Ernst, M. Matsuo, S.-I. Orimo and A. Züttel, *Journal of Physical Chemistry A*, 2011, **115**, 5329–5334.
- [47] J. A. Kilner and M. Burriel, *Ann. Rev. Mater. Res.*, 2014, **44**, 365–393.
- [48] L. Malavasi, C. A. J. Fisher and M. S. Islam, *Chem. Soc. Rev.*, 2010, **39**, 4370–4387.
- [49] M. Karlsson, *Phys. Chem. Chem. Phys.*, 2015, **17**, 26–38.

- [50] Y. Kobayashi, O. J. Hernandez, T. Sakaguchi, T. Yajima, T. Roisnel, Y. Tsujimoto, M. Morita, Y. Noda, Y. Mogami, A. Kitada, M. Ohkura, S. Hosokawa, Z. Li, K. Hayashi, Y. Kusano, J. eun Kim, N. Tsuji, A. Fujiwara, Y. Matsushita, K. Yoshimura, K. Takegoshi, M. Inoue, M. Takano and H. Kageyama, *Nat. Mater.*, 2012, **11**, 507–511.
- [51] B. Malaman and J. F. Brice, *J. Solid State Chem.*, 1984, **53**, 44–54.
- [52] N. J. Clark and E. Wu, *J. Less Common Metals*, 1988, **142**, 145–154.
- [53] B. Huang and J. D. Corbett, *Inorg. Chem.*, 1998, **37**, 1892–1899.
- [54] B. Huang and J. D. Corbett, *J. Solid State Chem.*, 1998, **141**, 570–575.
- [55] R. M. Helps, N. H. Rees and M. A. Hayward, *Inorg. Chem.*, 2010, **49**, 11062–11068.
- [56] K. Hayashi, S. Matsuishi, T. Kamiya, M. Hirano and H. Hosono, *Nature*, 2002, **419**, 462–465.
- [57] M. A. Hayward, E. J. Cussen, J. B. Claridge, M. Bieringer, M. J. Rosseinsky, C. J. Kiely, S. J. Blundell, I. M. Marshall and F. L. Pratt, *Science*, 2002, **295**, 1882–1884.
- [58] Y. Iwazaki, T. Suzuki, Y. Mizuno and S. Tsuneyuki, *Physical Review B - Condensed Matter and Materials Physics*, 2012, **86**, 214103–1 – 214103–6.
- [59] M. Schrader, D. Mienert, T.-S. Oh, H.-I. Yoo and K. Becker, *Solid State Sciences*, 2008, **10**, 768–775.
- [60] Y. Iwazaki, T. Suzuki and S. Tsuneyuki, *Journal of Applied Physics*, 2010, **108**, 083705–1 – 083705–7.
- [61] C. A. Bridges, F. Fernandez-Alonso, J. P. Goff and M. J. Rosseinsky, *Adv. Mater.*, 2006, **18**, 3304–3308.
- [62] A. Muntzer (NCNR), *Neutron scattering lengths and cross sections*, <https://www.ncnr.nist.gov/resources/n-lengths/>, accessed 2016-03-11.
- [63] *Neutron Applications in Earth, Energy and Environmental Sciences*, ed. L. Liang, R. Rinaldi and H. Schober, Springer: New York, 2009.

- [64] L. E. Smart and E. A. Moore, *Solid State Chemistry: An Introduction*, Taylor & Francis: Boca Raton, Third Edition edn., 2005.
- [65] D. Marquardt, R. J. Alsop, M. C. Rheinstädter and T. A. Harroun, *Journal of Cardiovascular Development and Disease*, 2015, **2**, 125–140.
- [66] T. Ramirez-Cuesta, P. Stewart and J. Tomkinson, *TOSCA User Manual*, <http://www.isis.stfc.ac.uk/instruments/tosca/documents/tosca-user-manual6685.pdf>, accessed 2016-04-21.
- [67] T. Yildirim, P. M. Gehring, D. A. Neumann, P. E. Eaton and T. Emrick, *Phys. Rev. B*, 1999, **60**, 314–321.
- [68] A. Remhof, P. Mauron, A. Züttel, J. P. Embs, Z. Łodziana, A. J. Ramirez-Cuesta, P. Ngene and P. de Jongh, *J. Phys. Chem. C*, 2013, **117**, 3789–3798.
- [69] J. R. D. Copley and J. C. Cook, *Chem. Phys.*, 2003, **292**, 477–485.
- [70] B. Kamitakahara, *DCS Design Features and Principal Specifications*, <http://ncnr.nist.gov/instruments/dcs/>, accessed 2016-04-04.
- [71] A. Meyer, R. M. Dimeo, P. M. Gehring and D. A. Neumann, *Review of Scientific Instruments*, 2003, **74**, 2759–2777.
- [72] T. Jenkins, *High Flux Backscattering Spectrometer*, <http://ncnr.nist.gov/instruments/hfbs/>, accessed 2016-04-04.
- [73] P. Stewart and R. Svemir, *TOSCA: A World Class Inelastic Neutron Spectrometer*, <http://www.isis.stfc.ac.uk/instruments/tosca/tosca4715.html>, accessed 2016-03-11.
- [74] S. F. Parker, F. Fernandez-Alonso, A. J. Ramirez-Cuesta, J. Tomkinson, S. Rudic, R. S. Pinna, G. Gorini and J. F. Castañon, *Journal of Physics: Conference Series*, 2014, **554**, 012003.
- [75] P. C. H. Mitchell, S. F. Parker, A. J. Ramirez-Cuesta and J. Tomkinson, *Vibrational Spectroscopy with Neutrons*, World Scientific: Singapore, 2005, vol. 3.

-
- [76] S. Emmanuelle, F. D. M. Teresa and R. Clemens, *D2B - High-resolution two-axis diffractometer*, <https://www.ill.eu/instruments-support/instruments-groups/instruments/d2b/description/instrument-layout/>, accessed 2016-03-11.
- [77] R. Eriksson, *ESS European Spallation Source*, <https://europeanspallationsource.se/>, accessed 2016-04-19.

